Available online at www.sciencedirect.com
SCIENCE DIRECT®
International Journal of Solids and Structures 43 (2006) 1528–1542
INTERNATIONAL JOURNAL OF SOLIDS and STRUCTURES
www.elsevier.com/locate/ijsolstr

# Fracture in metal powder compaction

S.M. Tahir [a,*], A.K. Ariffin [b]

[a] Department of Mechanical & Manufacturing Engineering, University Putra Malaysia, 43400 UPM Serdang, Selangor, Malaysia
[b] Department of Mechanical & Materials Engineering, University Kebangsaan Malaysia, 43600 Bangi, Selangor, Malaysia

Received 23 November 2004; received in revised form 6 September 2005
Available online 13 December 2005

**Abstract**

This paper presents a preliminary assessment and qualitative analysis on fracture criterion and crack growth in metal powder compact during the cold compaction process. Based on the fracture criterion of granular materials in compression, a displacement based finite element model has been developed to analyse fracture initiation and crack growth in metal powder compact. Approximate estimation of fracture toughness variation with relative density is established in order to provide the fracture parameter as compaction proceed. A single crack initiated from the boundary of a multi-level component made of iron powder is considered in this work. The finite element simulation of the crack propagation indicates that shear crack grows during the compaction process and propagates in the direction of higher shear stress and higher relative density. This also implies that the crack grows in the direction where the compaction pressure is much higher, which is in line with the conclusion made by previous researchers on shear crack growth in materials under compression. In agreement with reported work by previous researchers, high stress concentration and high density gradient at the inner corner in multi-level component results in fracture of the component during preparation.


*Keywords:* Powder compact; Fracture criteria; Shear crack; Finite element

## 1. Introduction

Powder metallurgy (PM) is widely applied to produce mainly automotive parts such as bearings, cams, and toothed components. Manufacturing parts using PM involves four major steps: powder and lubricant mixing, compacting powders into appropriate shapes in closed dies to produce green compacts, sintering the green compacts at elevated temperature and finally, post-sintering secondary operations (Chtourou et al., 2002; Mori et al., 1999).

In modelling the compaction process, the macro-mechanical modelling approach is used in this work, which provides information on the macroscopic behaviour of the powder assembly such as powder movement, density distribution, stress state and the shape of the compact during and after compaction. Thus the powder medium is considered as a continuum that undergoes large elastic–plastic deformation. In order to describe

* Corresponding author.
*E-mail address:* suraya_mtahir@yahoo.com (S.M. Tahir).

0020-7683/$ - see front matter © 2005 Elsevier Ltd. All rights reserved.
doi:10.1016/j.ijsolstr.2005.10.010

the effect of loading state on the response of the powder, constitutive model based on granular material is used since it was found in the literature that powder behaves similarly to a frictional granular material with regard to dilatancy and densification behaviour (Gollion et al., 1989). Details on cold compaction process can be found in Ariffin and Ihsan (1995), where the numerical modelling of the compaction, relaxation, ejection and emergence phases have been developed, and validated by experiments.

Based on the loading condition imposed on the powder material in a closed die, an extensive review on materials under compression is needed to determine the type of fracture that will most likely occur during the powder compaction process. The research reported in the literature has mainly focused on mode I fracture since experimental observations indicate that crack usually grows under pure opening mode before crack growth under mixed-mode or pure shear mode conditions. Even under pure shear loading, a crack generally grows under mode I due to the local tensile stresses at the crack tip. However, some researchers Melin (1986, 1987), De Bremaecker and Ferris (2004), Isaksson and Stahle (2002), Otsuka and Aoyama (1993), Liu (1974), Hallback (1998), Arun Roy et al. (1999) and Isaksson and Stahle (2003) have reported that crack grows under mode II condition when the confining pressure or compressive load is substantially high. In addition, the crack propagation pattern (or direction) generally depends on this confining pressure, or compressive load.

Experimental and numerical simulation results on crack growth in brittle materials (Melin, 1986, 1987; De Bremaecker and Ferris, 2004; Isaksson and Stahle, 2002) and ductile materials (Otsuka and Aoyama, 1993; Liu, 1974; Hallback, 1998; Arun Roy et al., 1999; Isaksson and Stahle, 2003) under compression indicate the same trend of crack propagation. Generally, crack can grow in three different manners:

i) under low pressure, crack grows via incipient kink by opening mode, at an angle from the original crack plane,
ii) under increasing pressure, crack grows as a combination of open (mode I) and shear (mode II) crack,
ii) under substantially high pressure, crack grows as a shear (mode II) crack, straight ahead or at a small angle from the original crack plane.

In all the referred experiments, a systematic examination of the influence of friction between the crack surfaces has not been analysed. However, Isaksson and Stahle (2003) in their analysis and computations have verified that apart from a high hydrostatic pressure, high friction between crack surfaces will suppress opening mode crack growth. At a sub-critical hydrostatic pressure or with lower friction between the crack surfaces, the crack can grows via a kink subjected to opening mode. The direction of the kink with respect to the original crack plane decreases with increasing pressure or increasing friction.

In granular materials like metal powder, the cohesive frictional behaviour of the material and inhomegeneity within the powder compact will have a significant influence on the type of fracture. Failure of metal powder during compaction has always been related to the shearing and friction behaviour of the material, where the yield criteria of powder material model have been developed based on soil mechanics material model (Chtourou et al., 2002; Ariffin and Ihsan, 1995). Therefore, it is believed that fracture in metal powder compaction most likely will be due to shear fracture, rather than opening fracture due to the mechanical behaviour of powder material in closed die compaction.

Unfortunately, to date there is no published materials on crack growth in soil mechanics for granular materials like sands or clays under compression, which might represent similar fracture behaviour as in metal powder. However, research on granular materials under compression has been carried out in rock mechanics (Yu et al., 2002; Rao et al., 2003; Bobet, 2000), which also shows a similar trend of crack propagation as mentioned above for fully dense brittle and ductile materials. Rocks can become more ductile when exposed to large confining pressure, where the stress–strain curve plotted from data derived from compression test on a rock sample as shown in Fig. 1 (Cal Poly Pomona, 2000) shows a similar behaviour to ductile materials. As the sample deforms, it passes through three different types of behaviours: elastic, ductile, and finally brittle failure, where cohesion is lost between the components of the rock.

Numerical simulations on powder compaction which focused on the stress and density distributions is insufficient in order to produce a crack free component since cracks are still formed in some green components, where methods for crack detection in green PM parts (Eric et al., 2003; Frederick, 2003) exist. The cracks in green parts are formed because either interparticle bonds are not formed or the interparticle bonds

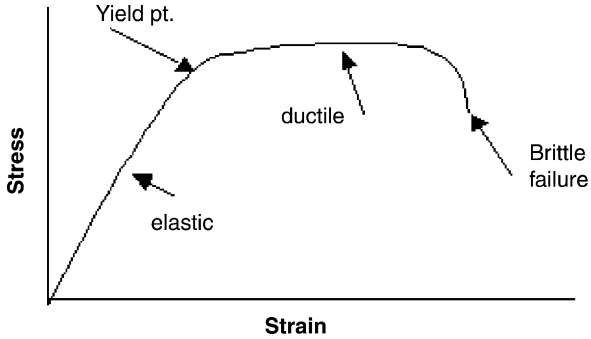


Fig. 1. Stress–strain behaviour of rock in compression.

become broken (Zenger and Cai, 1997). Due to the cohesive frictional behaviour of granular materials in compression, it is assumed in this work that it is possible for metal powder to undergo brittle failure when cohesion is lost between powder particles during the compaction process, as in rock materials under compression. Furthermore, from the three point bending test on iron powder compact by Poquillon et al. (2002), it was observed that fracture results from particle separation, where there is no difference in the fracture surface submitted to compression and the fracture surface submitted to tensile stress.

In this paper, a suitable fracture criterion for metal powder during cold compaction process is outlined, taking into accounts the mechanical behaviour of metal powder under compaction process. A displacement based finite element procedures has been developed to simulate the powder compaction and fracture process. Mohr–Coulomb yield criterion is used in this work, and FORTRAN programming language is utilised in developing the finite element procedures. An adaptive finite element mesh with error estimator based on stress error norm is used, while crack is modelled to propagate inter-element using the node release mechanism. Six nodes isoparametric elements are used as interface elements for friction between the powder material and the die wall during the compaction process, as well as to model friction on the crack faces in contact. This work aims to provide a preliminary assessment on fracture in metal powder compaction where further development can be carried out based on qualitative analysis of the simulation results presented in this paper.

## 2. Fracture criteria

Even though it is believed that failure in metal powder compaction is due to shear fracture (mode II), the fracture criterion in need must not neglect the possibility of fracture due to opening mode (mode I). Classical mixed mode fracture criteria have always been used to find the crack initiation angle (or direction) where crack extension depends on a specific fracture parameter. However, analysis by Rao et al. (2003) based on three basic criteria, namely the maximum circumferential stress criterion ($\sigma_\theta$-criterion) (Erdogan and Sih, 1963), the maximum strain energy release rate criterion ($G$-criterion) (Palaniswamy et al., 1972) and the minimum strain energy density criterion ($S$-criterion) (Sih, 1974), reveals that these criteria fail to predict the occurrence of mode II fracture even when pure shear load is applied. The crack initiation angle obtained from all three criteria is between $-70°$ and $-80°$ from the original crack plane when pure shear load is applied, while the true mode II crack should be in the direction of the maximum shear stress intensity factor, that is in the original crack plane (0°) or at a small angle from the original crack plane. In other words, the analysis proved that a more robust fracture criterion is needed to predict the occurrence of mode II crack.

Therefore, based on the examination of mode I and mode II stress intensity factors on the arbitrary plane $\theta$ based on the stress components near a crack tip as in Fig. 2, $K_{\mathrm{I}}(\theta)$ and $K_{\mathrm{II}}(\theta)$, varying with $\theta$ ($-180° \leqslant \theta \leqslant +180°$), no matter what kind of loading condition is applied, the fracture criterion (Rao et al., 2003) stated that for mode I fracture to occur:

$$1 < \frac{K_{\mathrm{II}\,\max}}{K_{\mathrm{I}\,\max}} < \frac{K_{\mathrm{IIC}}}{K_{\mathrm{IC}}}, \quad K_{\mathrm{I}\,\max} = K_{\mathrm{IC}} \quad \text{at } \theta_{\mathrm{IC}} \tag{1}$$

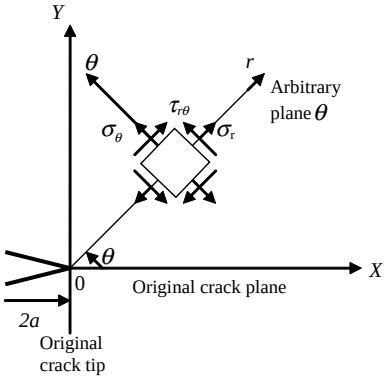


Fig. 2. Stress component at a point near a crack tip in the polar coordinate system.

For mode II fracture:

$$\frac{K_{\mathrm{II}\max}}{K_{\mathrm{I}\max}} > \frac{K_{\mathrm{IIC}}}{K_{\mathrm{IC}}}, \quad K_{\mathrm{II}\max} = K_{\mathrm{IIC}} \quad \text{at } \theta_{\mathrm{IIC}} \tag{2}$$

where $K_{\mathrm{I}\max}$ and $K_{\mathrm{II}\max}$ are the maximum stress intensity factors of mode I and mode II, respectively, while $K_{\mathrm{IC}}$ and $K_{\mathrm{IIC}}$ are the critical stress intensity factors of mode I and mode II. Details on calculation of stress intensity factors in the finite element model will be explained in the next section.

## 3. Finite element modelling of fracture in powder compact

### 3.1. Calculation of stress intensity factor (SIF)

In order to determine $K_{\mathrm{I}\max}$ and $K_{\mathrm{II}\max}$ in Eqs. (1) and (2), mode I and mode II stress intensity factors in the $\theta$ direction are defined as (Rao et al., 2003):

$$K_{\mathrm{I}}(\theta) = K_{\mathrm{I}}\cos^3\frac{\theta}{2} + K_{\mathrm{II}}\left(-\sin\frac{\theta}{2}\cos^2\frac{\theta}{2}\right) \tag{3}$$

$$K_{\mathrm{II}}(\theta) = K_{\mathrm{I}}\sin\frac{\theta}{2}\cos^2\frac{\theta}{2} + K_{\mathrm{II}}\cos\frac{\theta}{2}\left(1 - 3\sin^2\frac{\theta}{2}\right) \tag{4}$$

The crack initiation angles $\theta_{\mathrm{IC}}$ and $\theta_{\mathrm{IIC}}$, at which $K_{\mathrm{I}}(\theta)$ and $K_{\mathrm{II}}(\theta)$ reach the maximum $K_{\mathrm{I}\max}$ and $K_{\mathrm{II}\max}$ can be deduced from:

$$\frac{\partial K_{\mathrm{I}}(\theta)}{\partial\theta} = 0, \quad \frac{\partial^2 K_{\mathrm{I}}(\theta)}{\partial\theta^2} < 0 \tag{5}$$

$$\frac{\partial K_{\mathrm{II}}(\theta)}{\partial\theta} = 0, \quad \frac{\partial^2 K_{\mathrm{II}}(\theta)}{\partial\theta^2} < 0 \tag{6}$$

Alternatively, $K_{\mathrm{I}}(\theta)$ and $K_{\mathrm{II}}(\theta)$ are calculated on the mid nodes around the crack tip as shown in Fig. 3 to obtain the maximum $K_{\mathrm{I}\max}$ and $K_{\mathrm{II}\max}$, where $\theta$ is defined as positive in the anticlockwise direction from the original crack plane.

$K_{\mathrm{I}}$ and $K_{\mathrm{II}}$ in Eqs. (3) and (4) are the stress intensity factors in the original crack plane. In finite element method, these values can be calculated using the displacement correlation technique (Phan et al., 2003) as below:

$$K_{\mathrm{I}} = \frac{G}{\kappa+1}\sqrt{\frac{2\pi}{L}}\left(4(v_b - v_d) - \frac{(v_c - v_e)}{2}\right) \tag{7}$$

$$K_{\mathrm{II}} = \frac{G}{\kappa+1}\sqrt{\frac{2\pi}{L}}\left(4(u_b - u_d) - \frac{(u_c - u_e)}{2}\right) \tag{8}$$

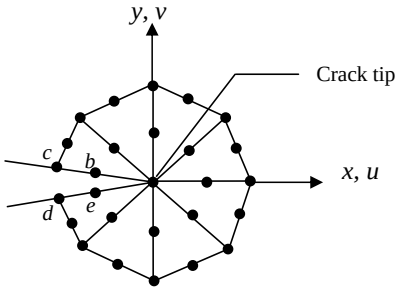


Fig. 3. Nodes around the crack tip for calculation of the stress intensity factors.

where $G$ is the shear modulus, $L$ is the element length, $\kappa$ is defined as $\kappa = (3 - 4v)$ for plane strain or axisymmetric problem, where $v$ is the Poisson's ratio. The $u$ and $v$ are the displacement components in $x$ and $y$ directions, respectively, where the subscripts indicate their positions as shown in Fig. 3.

### 3.2. Adaptive mesh and crack mechanism

An adaptive finite element mesh is applied to accommodate large displacement changes in geometry of the domain. Error estimator based on stress error norm (Zienkiewicz and Zhu, 1989) is used, where automatic remeshing is calculated at each step during the compaction process. Crack initiation and propagation have been developed and implemented in the model, without having to predefine the direction of crack. Initially, a three nodes triangle element is used. After the first stage of remeshing, the three nodes elements are automatically converted into six nodes triangle elements.

In finite element modelling using advanced remeshing technique, crack propagation can be modelled by inter-element or intra-element in the mesh (Bouchard et al., 2000). Since the values of $K_{\mathrm{I}}(\theta)$ and $K_{\mathrm{II}}(\theta)$ are calculated on the nodes around the tip, crack is modelled to propagate inter-element, while the node release mechanism (Bouchard et al., 2000) is used to provide two adjacent crack faces when the criteria is fulfilled. Using an adaptive mesh, the maximum and minimum element size can always be chosen such that the smallest element will be generated around the crack tip. As crack propagates, elements with appropriate size are generated around the crack tip, while the mid node of an element will become a new crack tip in order to ensure that the crack extension is within the process zone.

### 3.3. Friction criteria

When two surfaces are in contact, a criteria defining tangential stick or slip occurrence is needed. In general, friction criteria between two surfaces can be stated as

$$F_f(\tau, \sigma_n) = \begin{cases} < 0 & \text{stick} \\ = 0 & \text{slip} \end{cases} \tag{9}$$

Coulomb friction law which is often adopted in friction problems is used in this work, and is given by

$$F_f(\tau, \sigma_n) = \mid \tau \mid + \mu\sigma_N \tag{10}$$

where $\tau$ is the friction shear stress, $\sigma_N$ is the normal stress which should be compressive for friction to developed, and $\mu$ is the coefficient of friction.

Six nodes isoparametric elements are used as interface elements for friction between the powder material and the die wall during the compaction process. Details on the constitutive model of friction based on analogy with plasticity which is incorporated into the interface elements, can be found in Ariffin and Ihsan (1995). The interface elements are also used to model friction on the crack faces in contact. Using an adaptive finite element mesh, the interface element can be inserted automatically on the crack faces, whenever a crack starts and grows.

### 3.4. Geometry and boundary conditions of finite element model

A multi-level component, in this case a rotational flanged component, is modelled by an axisymmetric representation as shown in Figs. 4 and 5. Iron powder with material properties obtained from experimental work in Aidah (2001) as listed in Table 1, is compacted by bottom and top punch movements. Total displacement of the bottom punch, $d_b = 7.69$ mm while the top punch displacement, $d_t = 6.06$ mm at the end of compaction process. In this work, the compaction is performed in 20 steps movement of bottom and top punch, respectively, and in turn as shown in Fig. 5. This mean that a total displacement of 7.69 mm is first achieved when the bottom punch had finished a 20 steps movement (step 1–20), followed by a total displacement of 6.06 mm by the top punch after a 20 steps movement (step 21–40).

### 3.5. Fracture toughness

The fracture criterion in Eqs. (1) and (2) require values of the critical stress intensity factors, $K_{IC}$ and $K_{IIC}$ which are the material parameters and also called fracture toughness. Standard procedures exist for determination of fracture toughness for solids, such as three point bending test or four point bending test. However, the fracture toughness of the powder compact during the compaction process is not as simple as fully dense solids due to continuous rapid change of density and other material properties at each compaction step. Hence

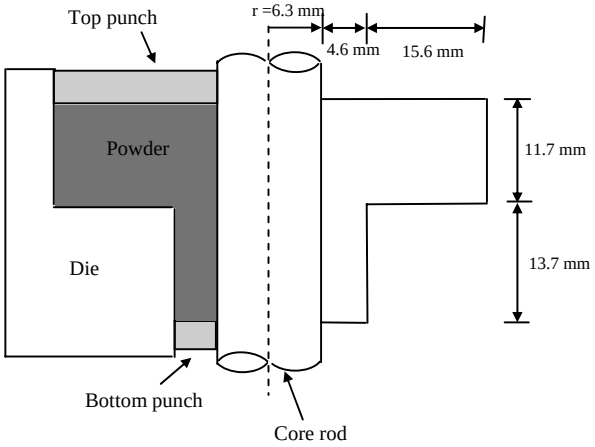


Fig. 4. Geometry and boundary conditions of a rotational flanged component.

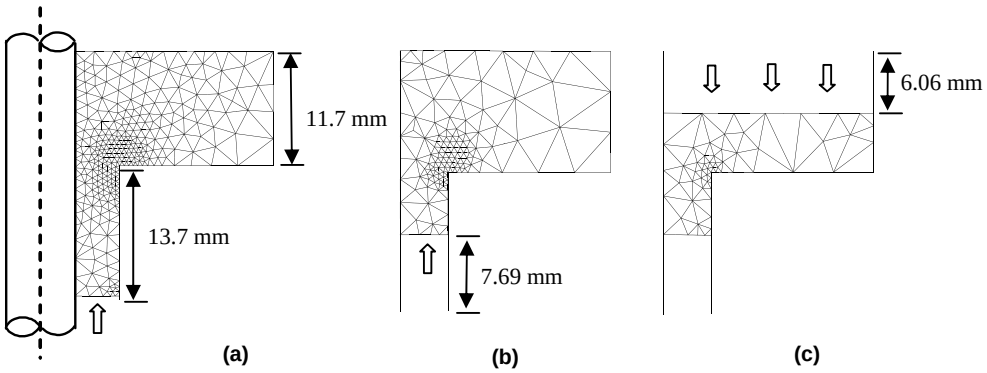


Fig. 5. Axisymmetric representation of compaction process with tool path and position during compaction process. (a) Step 1 begins, (b) end of step 20 and (c) end of step 40.

Table 1
Material properties of iron powder

| Material properties | |
|---|---|
| Young's modulus, $E$ | 40 MPa |
| Poisson ratio, $v$ | 0.35 |
| Cohesion, $C$ | 2.5 |
| Angle of internal friction, $\phi$ | 33 |
| Coulomb's friction coefficient, $\mu$ | 0.3332 |
| Initial relative density, $\rho_0'$ | 0.327 |

variation of fracture toughness with relative density must be obtained in order to provide these fracture parameters as compaction proceeds.

### 3.5.1. Mode I fracture toughness ($K_{IC}$)

Investigation on mechanical properties of iron compact has been carried out by Poquillon et al. (2002), who includes an analysis on different theoretical models to estimate variation of Young's modulus with relative density of the iron compact. In their work, the result obtained by assuming that green compacts behave as foam metal using the formulas given in Gibson and Ashby (1988) is comparable to the result obtained using the widely used assumption that green compacts behave as porous material. A detailed study on mechanical properties of foam is provided in Gibson and Ashby (1988) that includes approximate formulas for mode I fracture toughness ($K_{IC}$).

Therefore as a first approximation, the green compact is assumed to behave as foam metal in this work. Based on approximate formulas for mode I fracture toughness ($K_{IC}$) (Gibson and Ashby, 1988) and by assuming that the crack is parallel to one of the principal material axes, $K_{IC}$ can be estimated in the finite element simulation using the following formula (Choi and Sankar, 2003):

$$K_{IC} = \frac{\sigma_{US}}{\sigma_{max}} \tag{11}$$

where $\sigma_{US}$ is the strength of the material and $\sigma_{max}$ is the maximum principal stress.

Three point bending tests have been performed on iron compacts by Poquillon et al. (2002), where a number of samples with different final relative densities have been tested to provide the variation of green strength with relative density. A uniaxial press was used in the compaction process to produce the samples of iron compact and to analyse the densification behaviour of iron powder with different morphology (Poquillon et al., 2002). The effect of particle size and shape on the green strength is complex, but many studies carried out on metal powder compact green strength show that the green strength is a linear function of compaction pressure in a large range of relative density (Poquillon et al., 2002). Based on the densification behaviour of iron powder under uniaxial compaction by Poquillon et al. (2002) and Aidah (2001), as a first approximation in estimating $K_{IC}$, the variation of green strength with relative density obtained in Poquillon et al. (2002) as shown in Fig. 6 is used in this work. Using the variation of the green strength in Fig. 6, Eq. (11) hence becomes:

$$K_{IC} = \frac{148.66\rho' - 65.627}{\sigma_{max}} \tag{12}$$

where $\rho'$ is the relative density of the iron compact with respect to the solid iron, and $\sigma_{max}$ is the maximum principal stress as in Eq. (12).

### 3.5.2. Mode II fracture toughness ($K_{IIC}$)

The fracture toughness of a material is basically the amount of energy a material can absorb before fracture, or energy required to create new crack surfaces. Thus it is also equal to the area under the stress–strain curve up to fracture. Experimental data from shear box testing by Aidah (2001) is used in this work to obtain the shear stress–strain curves for samples of iron powder compact with different final compaction load (different final relative densities) as shown in Fig. 7. These curves are subsequently used to estimate the variation of

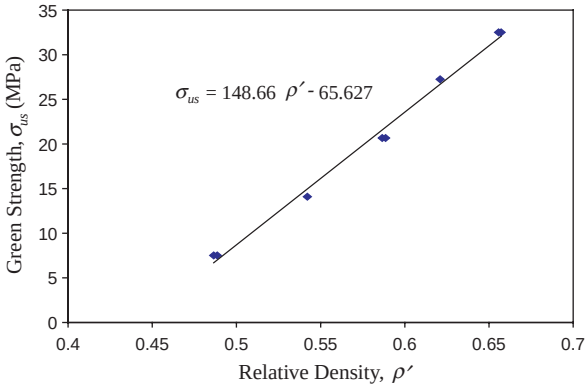


Fig. 6. Variation of green strength with relative density.

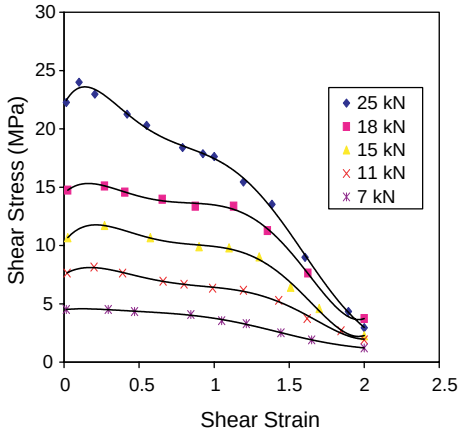


Fig. 7. Shear stress–strain curves for compacts with different final relative density compaction load.

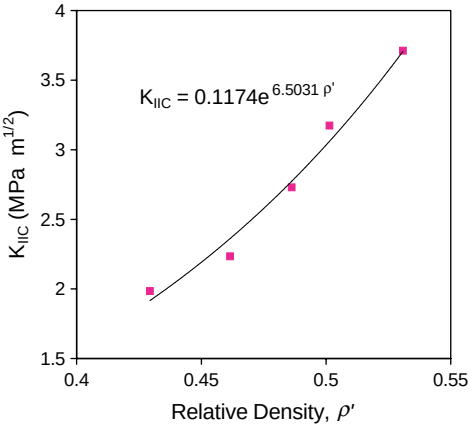


Fig. 8. Variation of $K_{IIC}$ with relative density.

mode II fracture toughness ($K_{IIC}$) with relative density, as depicted in Fig. 8. From Fig. 8, the values of $K_{IIC}$ as compaction proceeds can be obtained from:

$$K_{IIC} = 0.1174e^{6.5031\rho'} \tag{13}$$

where $\rho'$ is the relative density of iron compact as in Eq. (12). Since the crack is predicted to follow the direction of $K_{II\,max}$, the relative density at the point with maximum $K_{II}(\theta)$ around the crack tip is used in the calculation of both $K_{IC}$ and $K_{IIC}$.

## 4. Results and discussion

### 4.1. Crack initiation

Since no pre-crack is present in this case, the direction of maximum shear stress is used as the original crack direction, in the calculation of $K_I(\theta)$ and $K_{II}(\theta)$ for the first crack formation. This is acceptable because the same conclusions regarding the crack path are achieved in materials under compression, by assuming that crack grows along the plane of maximum shear stress as by assuming that crack follows the direction of maximum $K_{II}$ (Isaksson and Stahle, 2003). Without pre-crack in this work, the point with maximum shear stress is taken as the point where the crack starts.

A single crack propagating inward from the boundary surface is considered in this work. It is found that the point with the maximum shear stress is always generated around the sharp corner as shown in Fig. 9. Shear crack starts at the end of compaction step 9, and the shear stress distributions as well as the relative density distributions at step 10 are shown in Figs. 9 and 10, respectively. These two figures indicate that crack starts in the region with high shear stress but low relative density.

### 4.2. Crack propagation

As compaction proceeds, the crack propagates as shear crack at step 17, 18 and 20, where the crack propagation directions, $\theta$ at these steps are shown in Table 2. No further propagation occurs after step 20, until compaction is completed at step 40.

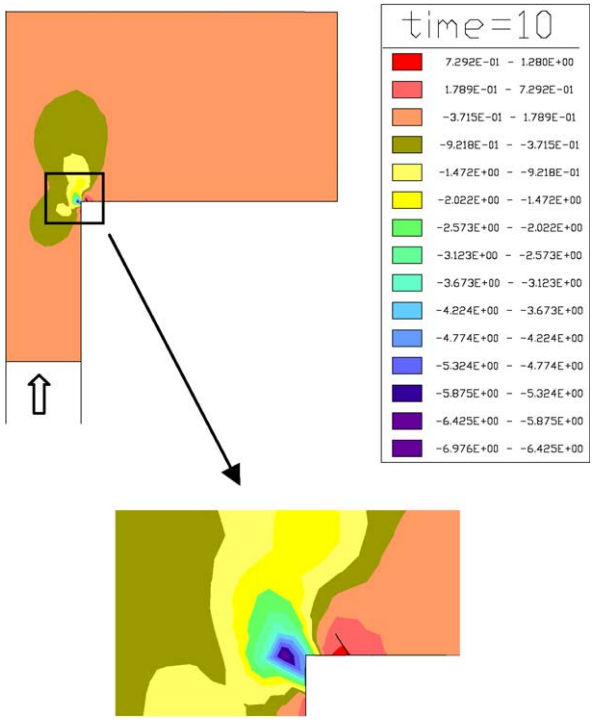


Fig. 9. Shear stress distribution at step 10.

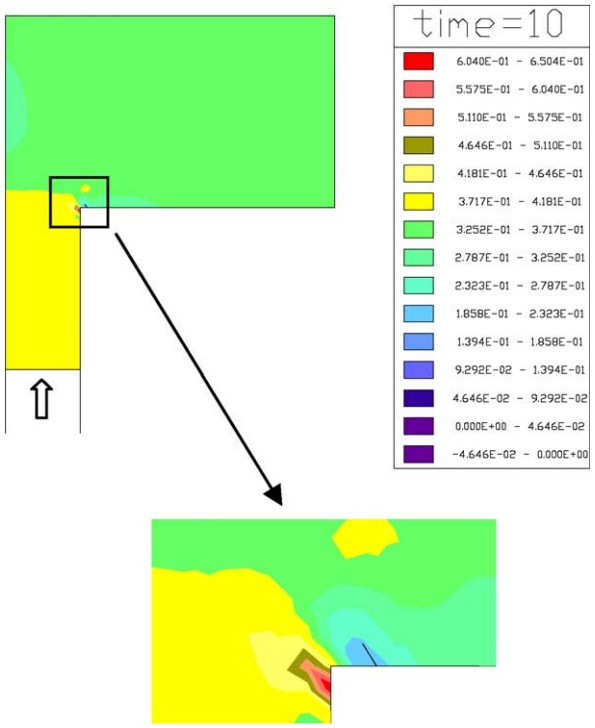


Fig. 10. Relative density distribution at step 10.

Table 2
Crack propagation direction

| Compaction step | $\theta$° |
|---|---|
| 17 | +22.7883 |
| 18 | +5.34889 |
| 20 | +13.74237 |

The value of $\theta$ is calculated with respect to the earlier crack direction and defined as positive in anticlockwise direction. These values of $\theta$ as listed in Table 2 show that the crack always extended away from the original crack direction and the crack propagation direction is relatively small compared to crack propagation direction reported in Liu (1974), Hallback (1998), Arun Roy et al. (1999), Isaksson and Stahle (2003) when crack extended via a kink by opening mode in materials under compression.

The shear stress distributions and relative density distributions at step 21 are shown in Figs. 11 and 12, respectively. Due to the small angle of propagation direction, a smooth curve of crack propagation is formed at the inner corner, showing the behaviour of shear crack growth. Neglecting the sign convention that indicates the direction of stresses, it can be seen from Fig. 11 that the crack propagates towards the region with higher shear stresses. Fig. 12 shows that the crack also propagates in the direction where the relative density is much higher. Since relative density increases as compaction pressure increases (Aidah, 2001; Poquillon et al., 2002), it can be deduced that the crack grows in the direction of higher compaction pressure. This is in line with the conclusion made by Arun Roy et al. (1999) arguing that crack grows in the direction of higher confining hydrostatic pressure, which is equivalent to the compaction pressure in this case.

Due to the movement of the bottom punch in the first 20 steps, the two regions with the highest and lowest relative density are formed around the inner corner as shown in Fig. 12. The relative density or compaction

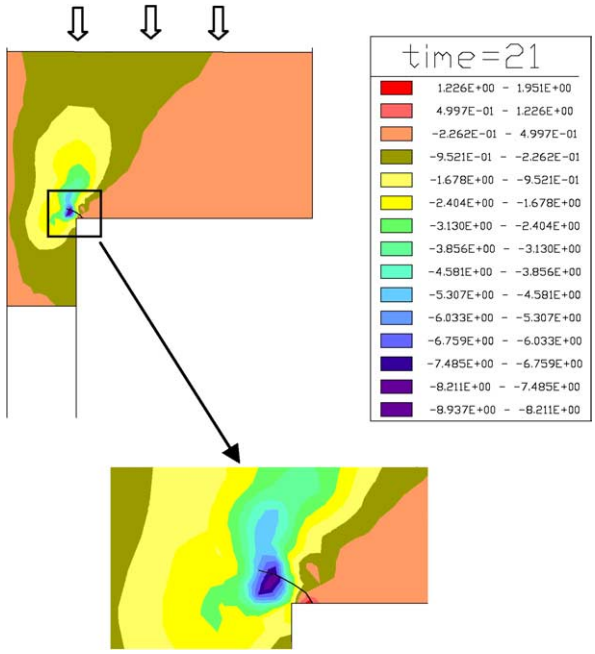


Fig. 11. Shear stress distribution at step 21.

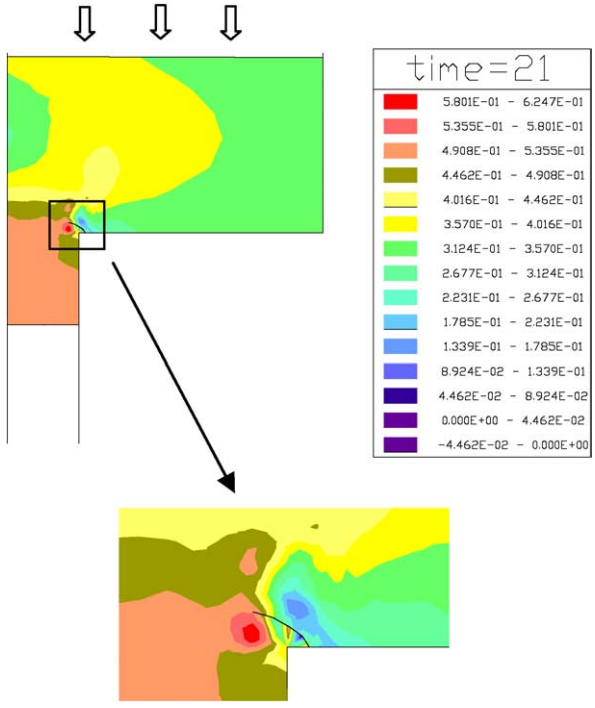


Fig. 12. Relative density distribution at step 21.

pressure gradient around the sharp corner causes the crack to propagate in such direction as in Fig. 12. Furthermore, the shear stresses which are initially higher at the boundary as shown in Fig. 9 become much lower

as compaction proceeds, while the region with higher shear stresses is formed slightly centred, at the inner corner as in Fig. 11. As the consequence, the crack propagates inward starting from the boundary, towards the region where the shear stresses are much higher. This is in agreement with reported fracture in multi-level component during preparation, expected to be caused by high stress concentration and high density gradient at inner corner (Mori et al., 1999; Oliver et al., 1996; Chtourou et al., 2002).

### 4.3. Example of fracture in metal powder compaction

To date the in situ observation on fracture during the compaction process is unattainable, where the cause of fracture is usually predicted based on the fractured part of the ejected green component (Mori et al., 1999; Chtourou et al., 2002). Even though it is of high interest to actually observe the fracture during the powder compaction process of engineering multi-level component which usually fracture near the inner corner, a simple component is produced in this work to provide an example of fracture in iron powder compact. This is due to limited available tools currently in the authors' laboratory to produce a real engineering multi-level

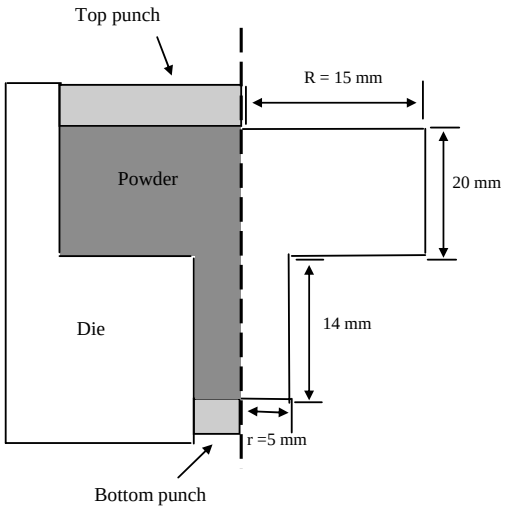


Fig. 13. Initial geometry and boundary condition of a simple component.

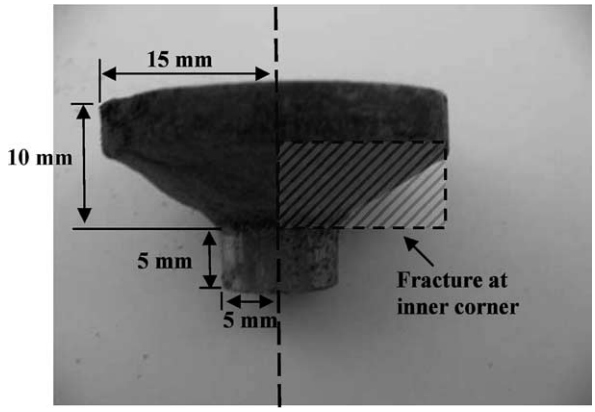


Fig. 14. Fracture at inner corner of a simple component.

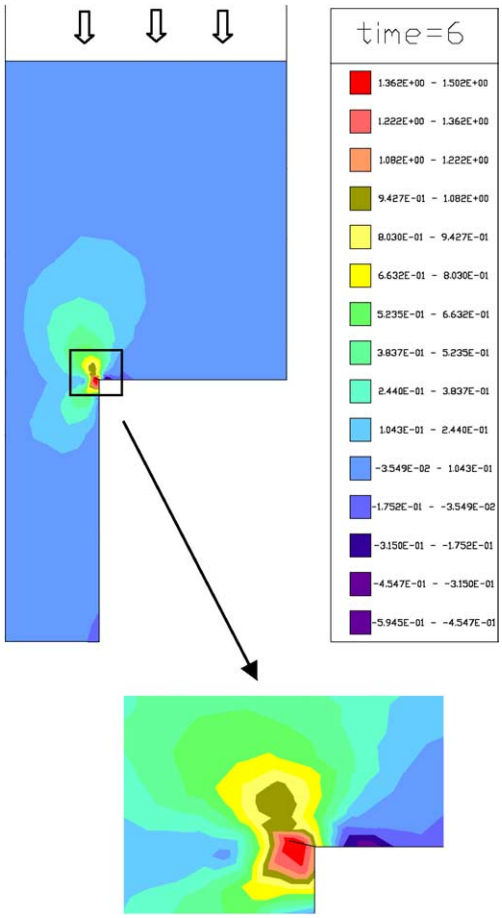


Fig. 15. Shear stress distribution at step 6.

component. Initial geometry and boundary condition of the component is shown in Fig. 13. Compaction is performed by downward movement of the top punch until a displacement of 10 mm is achieved, followed by upward movement of the bottom punch until a displacement of 9 mm is achieved. The final dimension of the component is as shown in Fig. 14, where it can be seen that fracture occurs in the lower region of the component, resulting in undesirable shape of the component.

Finite element simulation of the compaction process for this simple component is carried out for comparison purposes. Compaction by the movement of top and bottom punches is performed in 20 steps movement, respectively, similar to the simulation performed in Section 3.4 except that the top punch move first, followed by the bottom punch movement. For this component, simulation shows that crack starts at the end of step 5, where the shear stress and relative density distribution at step 6 are shown in Figs. 15 and 16, respectively. From these two figures, crack starts at inner corner of the component due to high shear stress concentration and high density gradient, as in the results of simulation presented in Section 4.1. However, crack does not propagate until the simulation of the compaction process is completed at step 40.

Comparing the results of simulation with the fracture in the component as shown in Fig. 14, it is believed that crack starts at the inner corner and causes the lower region of the component to fracture during ejection of the component from the die. Since effect of ejection on crack growth in the compact has not been analysed in this work, comparison can only be made on the point of fracture. Both simulation and experimentally produced component shows that fracture occur at the inner corner of the component resulting in a serious damage to the component.

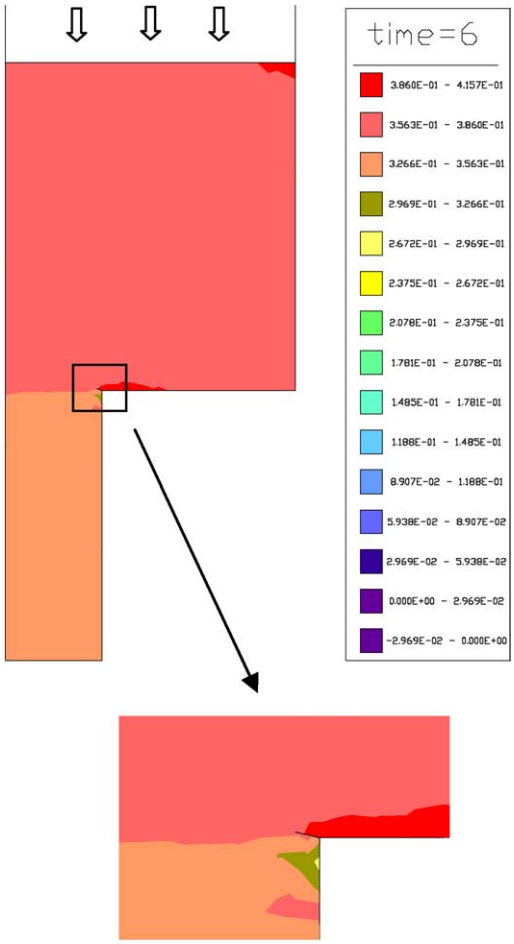


Fig. 16. Relative density distribution at step 6.

## 5. Conclusion

A displacement based finite element model has been developed to simulate the crack initiation and propagation in a rotational flanged component made of iron powder. A fracture criterion based on fracture of granular materials in compression has been successfully used to model the crack propagation process. Simulation of the crack propagation process in the iron compact shows that shear crack starts in the region with the highest shear stress and the lowest relative density distributions. As compaction proceeds, the crack propagates in shear mode in the direction where the shear stress and the relative density are much higher. Propagation of the crack towards the region of much higher relative density distribution also implies that the crack grows in the direction of higher compaction pressure, which is in line with the conclusion made by previous researchers on crack growth in materials under compression.

In addition, simulation of crack growth at inner corner in multi-level component due to high stress concentration and high density gradient around the corner is indeed in line with reported fracture in multi-level component during preparation by previous researchers. This useful preliminary assessment on fracture behaviour in metal powder during the compaction process can be further developed for prediction of crack growth in multi-level components with more complex geometrical shape and by using more accurate material fracture parameters.

## References


Aidah J., 2001. Analysis of Thermo-Mechanical Behaviour of Warm Compaction Process (In Malay Language), Master of Science Thesis, Universiti Kebangsaan Malaysia, Malaysia.

Ariffin, A.K., Ihsan, M., 1995. Powder Compaction, Finite Element Modelling and Experimental Validation, Ph.D. Thesis. University of Wales Swansea, United Kingdom.

Arun Roy, Y., Narasimhan, R., Arora, P.R., 1999. An experimental investigation of constraint effects on mixed mode fracture initiation in a ductile aluminium alloy. Acta Mater. 47, 1587–1596.

Bobet, A., 2000. The initiation of secondary cracks in compression. Eng. Fracture Mech. 66, 187–219.

Bouchard, P.O., Bay, F., Chastel, Y., Tovena, I., 2000. Crack propagation modelling using an advance remeshing technique. Comput. Methods. Appl. Mech. Eng. 189, 723–724.

Cal Poly Pomona, 2000. Properties of Rocks Under Stress. Structural Geology. Available from: <http://geology.csupomona.edu/alert/default.htm>.

Choi, S., Sankar, B.V., 2003. Fracture toughness of carbon foam. J. Compos. Mater. 37 (23), 2101–2116.

Chtourou, H., Guillot, M., Gakwaya, A., 2002. Modelling of the metal powder compaction process using the cap model. Part 1: Experimental material characterisation and validation. Int. J. Solids Struct. 39, 1059–1075.

Chtourou, H., Gakwaya, A., Guillot, M., 2002. Modeling of the metal powder compaction process using the cap model. Part II. Numerical implementation and practical applications. Int. J. Solids Struct. 39, 1077–1096.

De Bremaecker, J.Cl., Ferris, M.C., 2004. Numerical models of shear fracture propagation. Eng. Fracture Mech. 71, 2161–2178.

Erdogan, F., Sih, G.C., 1963. On the crack extension in plate under in-plane loading and transverse shear. J. Basic Eng. 85 (4), 519–527.

Eric, T.H., Rose, J.L., Song, W.-J, Heaney, D.F., 2003. A surface wave mediator technique for crack detection in green parts. In: Proceeding of the 2003 International Conference on Powder Metallurgy & Particulate Materials.

Frederick, K., 2003. Zetec, Inc., Eddy current testing of powder metal components. Available from: <www.zetec.com/documents/pwdr_met_Insp(1).pdf>.

Gibson, L.J., Ashby, M.F., 1988. Cellular Solids: Structure and Properties, second ed. Cambridge University Press, Cambridge, United Kingdom.

Gollion, J., Bouvard, D., Stutz, P., 1989. On the rheology of metal powder during cold compaction. In: J. Biarez, R. Gourves (Eds.), Proc. Int. Conf. Micromechanics of Granular Media, Powder and Grains, pp. 433–438.

Hallback, N., 1998. Mixed mode I/II fracture behaviour of a high strength steel. Int. J. Fract. 87, 363–388.

Isaksson, P., Stahle, P., 2002. Mode II crack paths under compression in brittle solids—A theory and experimental comparison. Int. J. Solids Struct. 39, 2281–2297.

Isaksson, P., Stahle, P., 2003. A directional crack path criterion for crack growth in ductile materials subjected to shear and compressive loading under plane strain conditions. Int. J. Solids Struct. 40, 3523–3536.

Liu, A.F., 1974. Crack growth failure of aluminium plate under in-plane shear. AIAA J. 12, 180–185.

Melin, S., 1986. When does a crack grow under mode II conditions? Int. J. Fract. 30, 103–114.

Melin, S., 1987. Fracture from a straight crack subjected to mixed-mode loading. Int. J. Fract. 32, 257–263.

Mori, K., Sato, Y., Shiomi, M., Osakada, K., 1999. Prediction of fracture generated by elastic recoveries of tools, in multi-level powder compaction using finite element simulation. Int. J. Machine Tools Manuf. 39, 1031–1045.

Oliver, J., Oller, S., Cante, J.C., 1996. A plasticity model for simulation of industrial powder compaction processes. Int. J. Solids Struct. 33 (20-22), 3161–3178.

Otsuka, A., Aoyama, M., 1993. Mode II fatigue under a compressive stress field: a simplified model for rolling contact. In: Rossmanith H.P., Miller K.J. (Eds.), Mixed-Mode Fatigue and Fracture ESIS 14, Mechanical Engineering, London, pp. 49–60.

Palaniswamy, K., Knauss, W.G., 1972. Propagation of a crack under general in-plane tension. Int. J. Fract. Mech. 8, 114–117.

Phan, A.V., Napier, J.A.L., Gray, L.J., Kaplan, T., 2003. Stress intensity factor analysis of friction sliding at discontinuity interfaces and junctions. Comput. Mech. 32 (4-6), 392–400.

Poquillon, D., Baco-Carles, V., Tailhades, Ph., Andrieu, E., 2002. Cold compaction of iron powders—Relations between powder morphology and mechanical properties. Part II. Bending tests: results and analysis. Powder Technol. 126, 75–84.

Poquillon, D., Lemaitre, J., Baco-Carles, V., Tailhades, Ph., Lacaze, J., 2002. Cold compaction of iron powders—Relations between powder morphology and mechanical properties. Part I: Powder preparation and compaction. Powder Technol. 126, 65–74.

Rao, Q., Sun, Z., Stephansson, O., Li, C., Stillborg, B., 2003. Shear fracture (mode II) of brittle rock. Int. J. Rock Mech. Mining Sci. 40, 355–375.

Sih, G.C., 1974. Strain energy density factor applied to mixed mode crack problem. Int. J. Fract. 10, 305–321.

Yu, M.H., Zan, Y.-W., Zhao, J., Mitsutoshi, Y., 2002. A unified strength criterion for rock material. Int. J. Rock Mech. Mining Sci. 39, 975–989.

Zenger, D.C., Cai, H., 1997. Handbook of the Common Cracks in Green P/M Compacts. Metal Powder Industries Federation, Princeton: NJ.

Zienkiewicz, O.C., Zhu, J.Z., 1989. Error estimates and adaptive refinement for plate bending problems. Int. J. Numer. Meth. Eng. 28, 2839–2853.